CAE Analysis of Spinning Conditions and Deformation Behavior of Automotive Exhaust Parts

OZAKI Yoshihiro*1 ISHIWATARI Akinobu*2 TAMAI Yoshikiyo*3

Abstract:

Experiments were conducted on pipe diameter reduction of automotive exhaust parts, such as catalytic converters and sub-mufflers by spinning process with ferritic stainless steels. Effects of several forming factors on the geometrical property and defects of the parts are clarified. The computer aided engineering (CAE) simulation model for spinning was also developed. Calculated results were in good agreement with actual spinning formed specimens not only in thickness distribution but also in shape of buckling defect. The results suggest that CAE simulation could be a helpful tool to obtain optimum forming conditions.

1. Introduction

The spinning forming process is an incremental forming method in which a stylus or roller tool push against the surface of the rotating workpiece. In recent years, an increasing number of automotive exhaust parts such as catalytic converter cases and muffler shells have been produced by numerically controlled (NC) spinning forming by reducing the diameter of the end of a ferritic stainless steel pipe [1–6]. The development of tool rotation type spinning forming method using a rotating tool and a fixed workpiece has made it possible to form not only parts with axial symmetric shapes but also eccentric or oblique axis shapes, thereby expanding the degree of freedom in part design [7–9]. On the other hand, there is also tendency to use thinner starting materials for weight reduction. But when thin materials with a thickness of 1.2 to 1.5 mm or less are used, cracking and buckling come to be viewed as a problem in spinning forming[10, 11]. Against this background, the aim of this study is to clarify the effects of complicated condition parameters of spinning forming on thickness distribution and the geometrical property.

2. Uni-Axial Symmetric Spinning

2.1 Method of Uni-Axial Symmetric Spinning Experiment

Figure 1 shows a schematic drawing of the configuration of the spinning forming process used in this study. That is the tool rotation type spinning forming method with two roller tools. The sample materials were two types of ferritic stainless steel, Steel A:

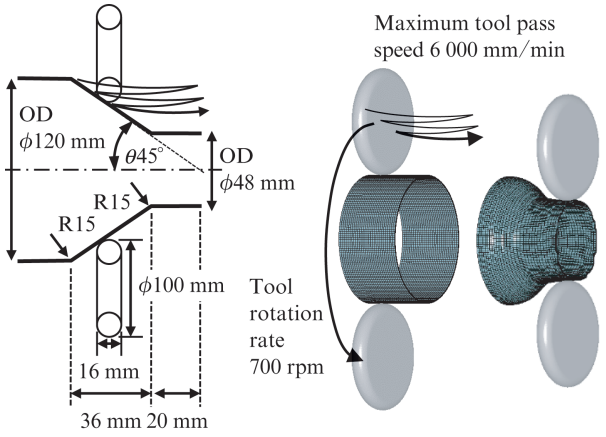

Fig. 1 Schematic drawing of configuration of tool rotation type spinning

† Originally published in *JFE GIHO* No. 48 (Aug. 2021), p. 41−47

*1 Senior Researcher Manager,
Forming Technology Research Dept.,
Steel Res. Lab.,
JFE Steel

*2 Dr. Eng.,
Senior Researcher Deputy General Manager,
Forming Technology Research Dept.,
Steel Res. Lab.,
JFE Steel

*3 Dr. Eng.,
General Manager,
Forming Technology Research Dept.,
Steel Res. Lab.,
JFE Steel

Table 1 Mechanical property of stainless steel for spinning experiment

	Thickness (mm)	0.2%PS (MPa)	TS (MPa)	El (%)	*n*-value (5-10%)	*r*-value (at 15%)
Steel A (JFE439L)	1.15	300	441	37	0.22	1.65
Steel B (JFE429EX)	1.51	324	478	39	0.22	1.60

Table 2 Experimental conditions for uni-axial symmetric spinning

Condition No.	Number of tool pass	Tool rotation rate (rpm)	Taper angle (degree)
① (Base)	19	700	45
②	19	600	45
③	19	500	45
⑥	37	700	45
⑦	25	700	45
⑧	15	700	45
⑨	13	700	45
⑲	19	700	35
⑳	19	700	55

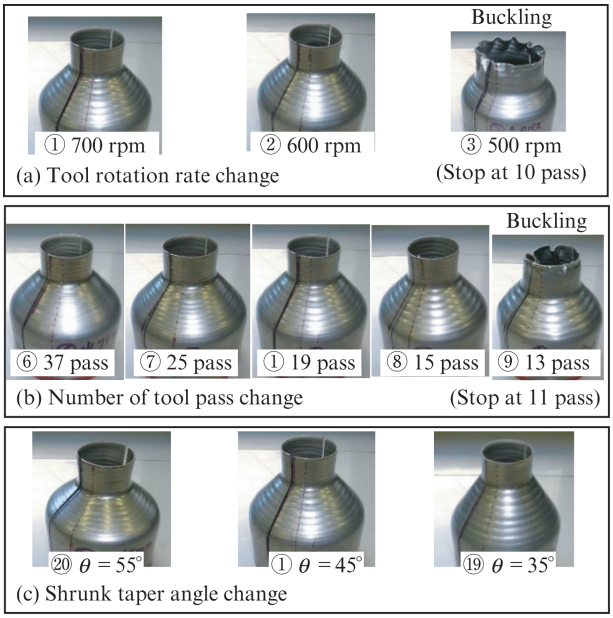

Fig. 2 Appearance of uni-axial symmetric spinning formed specimen

JFE439L (SUS430LX, 18% Cr-0.3% Ti) and Steel B: JFE429EX (Type 429, 15% Cr-0.4%Nb), both of which are the materials used in automotive exhaust parts. **Table 1** shows the mechanical properties of the sample steels. The low pipe material with outer diameter of φ120 mm are prepared using TIG (tungsten inert gas) welding technique. Uni-axial symmetric spinning forming was performed with a standard target shape having an outer diameter φ48 mm (diameter reduction ratio: 60%) at the pipe end, a taper shoulder angle of 45° and a shrunk neck length of 20 mm, assuming an automotive exhaust part. The base condition was Condition ① in **Table 2**, and the samples formed at various tool rotation rates, numbers of tool passes and taper shoulder angles are compared.

2.2 Results of Uni-Axial Symmetric Spinning Experiment

Figure 2 shows the appearance of the samples formed by uni-axial symmetric spinning using Steel A as the starting pipe. **Figure 3** shows the thickness distribution measured in the longitudinal direction, and **Fig. 4** shows the minimum thickness values.

2.2.1 Effect of tool rotation rate

Fig. 2 (a) and Fig. 3 (a) shows the appearance and thickness distribution of samples formed with different tool rotation rates, respectively. No remarkable differences were seen at the condition of 700 rpm and 600 rpm. However, under the low tool rotation rate of 500 rpm (Condition ③), buckling occurred at the pipe end, and forming was stopped in the 10th pass before forming was completed. In the spinning forming process, the rotating tools travel in a spiral locus while in contact with the surface of the pipe material. Since the tool travel distance is proportional to the rotation rate, it is thought that buckling occurred at the low rotation rate because the pipe diameter was reduced rapidly with a short tool travel distance.

2.2.2 Effect of number of tool passes

Fig. 2 (b) and Fig. 3 (b) show the appearance and thickness distribution of the samples, respectively, when the number of tool passes was changed. The smaller the number of tool passes was, the more remarkable the roller tool marks at the taper shoulder portion became. Comparing the thickness distributions (Fig. 3), as the number of tool passes increased, thickness reduction tended to be suppressed, but the effect on the minimum thickness value was unclear (Fig. 4). It is thought that decreasing the number of tool passes, the roller tools push the workpiece more strongly with an increased shrinking amount in each pass made the elongation of longitudinal direction, resulting in a thinner thickness. Under Condition ⑨, the number of passes was reduced to 13, the buckling occurred at the pipe end, and the experiment was stopped at the 11th

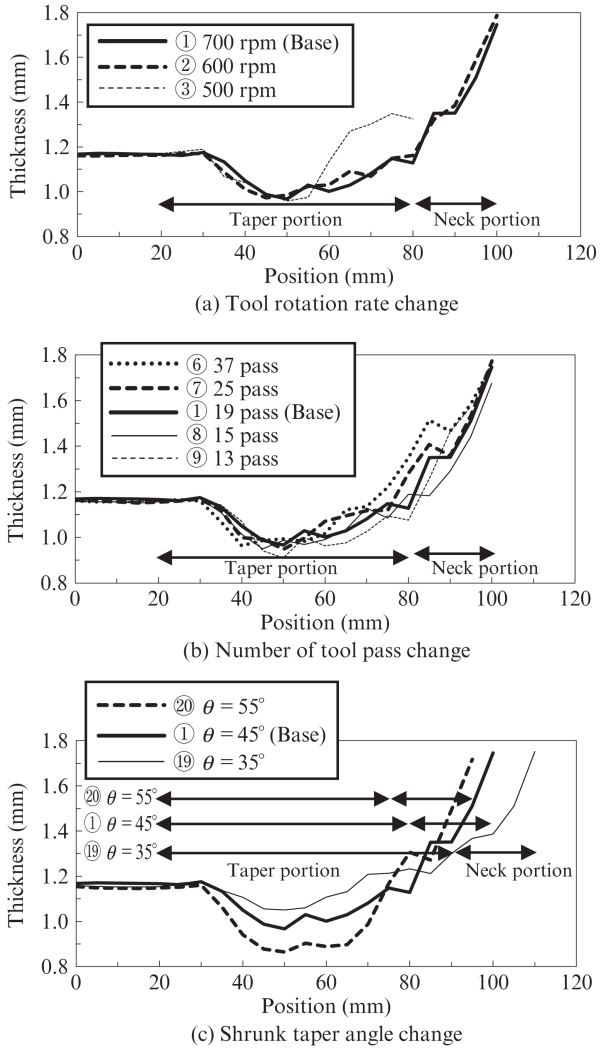

Fig. 3 Thickness distribution of uni-axis symmetric spinning formed specimen

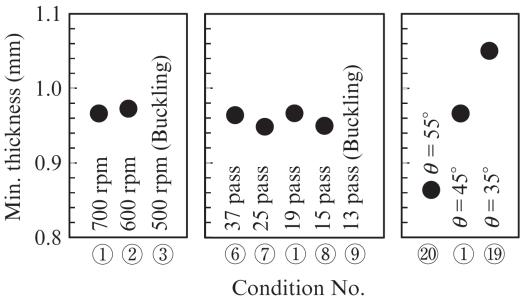

Fig. 4 Minimum thickness of uni-axis symmetric spinning formed specimen

pass, before forming was completed. As in the case of Condition ③ in the above Fig. 2 (a), this buckling is considered to be the result of a rapid reduction of the diameter with a shortened tool travel distance because of the small number of tool passes. In comparison with Condition ① (base condition, 700 rpm, 19 pass), the ratio of the travel distance were 500 rpm / 700 rpm = 0.71 in Condition ③ (low tool rotation rate of 500 rpm), and 13 passes / 19 passes = 0.68 in Condition ⑨ (reduced number of tool passes 13 pass). Therefore, it is considered that buckling occurs when the travel distance is shortened to approximately 0.7 times the Base condition.

2.2.3 Effect of taper angle

Fig. 2 (c) and Fig. 3 (c) show the appearance and thickness distribution of the samples, respectively, when the taper angle was changed. Here, it can be understood that both the thickness distribution (Fig. 3) and the minimum thickness (Fig. 4) decreases remarkably at the taper shoulder portion, as the taper angle is increased. Spinning forming involves the action of thickness increase by diameter reduction, and also involves the action of thickness decrease by elongation for the longitudinal direction. Assuming the target reducing diameter is the same, the larger the taper angle is, the larger the elongation ratio in the axial direction is, and consequently, the thickness of the taper portion is reduced.

2.3 Guidelines for Optimization of Spinning Conditions

Based on the experimental results presented above, it was found that the effects of the spinning forming conditions on the thickness distribution and geometrical property are as follows.

- Buckling occurs in condition of the tool rotation rate is low excessively.
- Buckling occurs in condition of the number of passes is decreased excessively.
- Thickness reduction is suppressed as the number of tool passes is increased.
- Thickness reduction is decreased as the taper angle becomes smaller.

3. FEM Simulation

3.1 FEM Modelling of Spinning Forming Process

Dynamic explicit FEM (Finite Element Method) simulation using Hill's yield function of the uniaxial symmetric spinning shown in Figure. 1 was carried out using a commercial solver, LS-DYNA™. The stress-strain curve of the material was modelled by Swift's formula, and it was calibrated based on the result of tensile test at room temperature of the specimens machined from a row pipe.

The roller tools were modelled with rigid shell elements, and the workpiece of a row pipe was modelled with deformable solid elements stacking 5 elements in

the thickness direction. In the FEM simulation, the row pipe was fixed, and the tools rotating around the formed pipe traveled back and forth along the pipe axis approaching to the axis the same as the hardware experiment as seen in Figure 1.

3.2 Results of FEM Simulation: Buckling of Pipe End

In **Figure 5**, the results of the FEM simulation are compared with the actual samples obtained in the experiments under Conditions ① and ③ of Table 2. Under Condition ①, the FEM results show slight waves at the pipe end, but are similar to the experimental results at a satisfactory level. Under Condition ③, the FEM simulation could duplicate severe buckling at the pipe end due to the low tool rotation rate as seen in the experiment. It can be said that the FEM simulation has good agreement with the experiment as to buckling tendency.

3.3 Results of FEM simulation: Change of Thickness Distribution

Figure 6 shows the comparison of thickness distribution along the longitudinal direction between FEM and experimental results, after the 8th, 12th, 16th, and 19th (final) passes under Condition ① of Table 2. The FEM simulation shows good agreement with the experiment as to the thickness distribution and its transition from early pass to the final pass.

The thickness of the tapered shoulder portion is smaller than the chucked base area which is not formed because of the elongation along the longitudinal direction. As the forming proceeds, the thickness reduction progresses toward the formed pipe end. On the other hand, the thickness of the formed pipe end portion is much thicker than the chucked base area due to the diameter reduction.

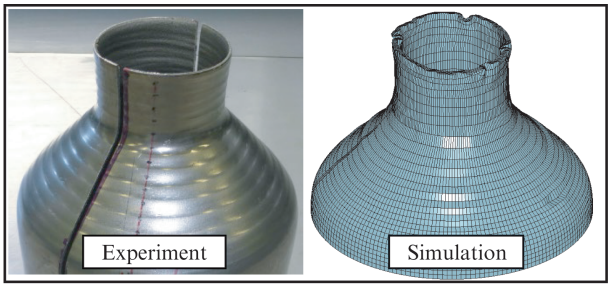

(a) Condition ①: Tool rotation 700 rpm

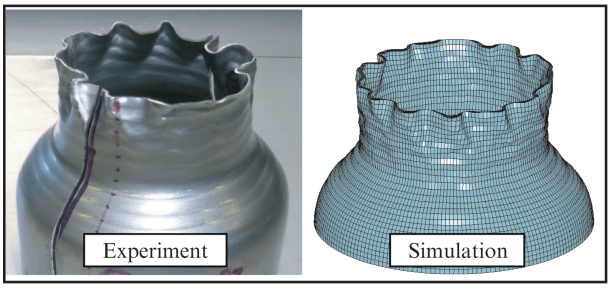

(b) Condition ③: Tool rotation 500 rpm
(Buckling arose, stopped at 10 pass)

Fig. 5 Comparison of calculated result shape with experimental specimen

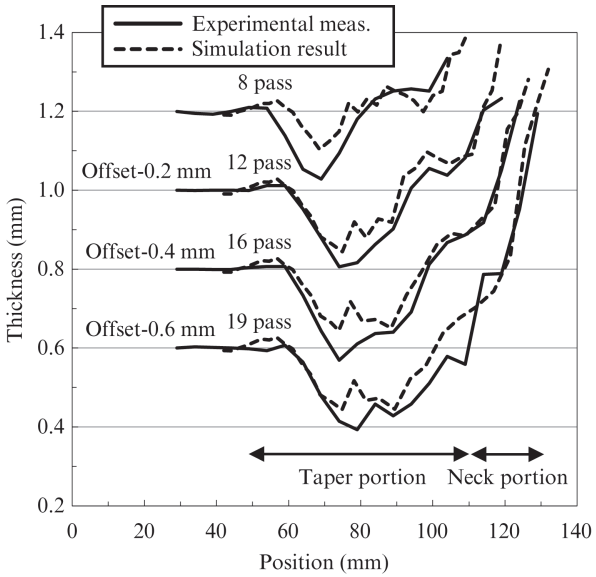

Fig. 6 Thickness distribution in each pass of uni-axis symmetric spinning formed specimen

4. Eccentric and Oblique Axis Spinning

4.1 Thickness Distribution by Eccentric and Oblique Axis Spinning

Figure 7 illustrates uniaxial symmetric spinning and diagonal spinning. The distinctive feature of the eccentric and oblique axis spinning is a shifted and tilted spinning axis as seen in Figure 7 (b). Asymmetric shapes like **Figure 8** (b) cannot be formed by conventional spinning adopting workpiece rotation. The eccentric and oblique axis spinning in this study can form the asymmetric shapes by shifting and tilting the axis of tool orbiting from the central axis of the formed pipe.

Eccentric and oblique axis spinning experiments under Condition ㉔ and ㉕ in **Table 3** were conducted using Steel A and B of Table 1, and the results were compared with uni-axial symmetric spinning experiment under Condition ①. The outer pipe diameter was reduced from initial φ120 mm to final φ48 mm (reduction ratio of 60%) as shown in section 2.1. The appearances of the formed samples and the thickness distributions measured in the direction of the largest taper angle θ (see Figure 7) are shown in Figure 8 and **Figure 9**, respectively. Although the direct comparison

Table 3 Experimental conditions for eccentric and oblique axis spinning

Condition No.	Number of tool pass	Tool rotation rate (rpm)	Taper angle (deg.)	Neck length (mm)	Tool rotation axis	
					Tilt (deg.)	Shift (mm)
① (Base)	19	700	45	20	0	0
㉔	75	700	52.5	20	15	25
㉕	75	700	57.4	20	15	35

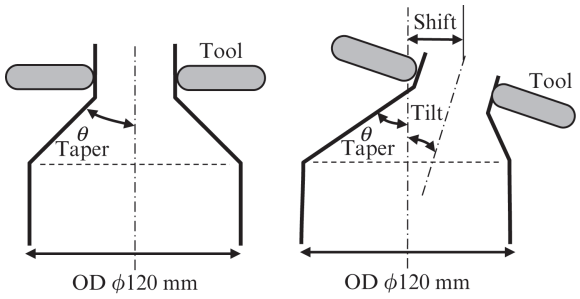

(a) Uni-axis symmetric spinning (b) Eccentric and oblique axis spinning

Fig. 7 Schematic drawing of configuration of tool rotation type spinning

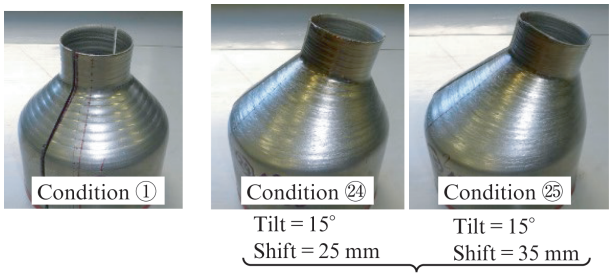

(a) Uni-axis symmetric spinning (b) Eccentric and oblique axis spinning

Fig. 8 Appearance of spinning formed specimen

between the two spinning methods is difficult because of the differences in tool movement and forming time, it appears that the minimum thickness in the taper shoulder portion is smaller by eccentric and oblique axis spinning than by axial symmetric spinning. While 19 tool passes were used in the uni-axial symmetric spinning of Condition ①, the eccentric and oblique axis spinning of Condition ㉔ and ㉕ needed 75 passes. The maximum taper angle θ of the eccentric and oblique axis spinning experiment was large: 52.5° under Condition ㉔, and 57.4° under Condition ㉕. That means the deformation in the eccentric and oblique axis spinning is partly very severe, as the amount of the pipe end movement at the maximum taper angle can be equivalent to a diameter reduction ratio of 100% or more. The tendency that the thickness reduction in the taper shoulder portion at the maximum taper angle is large in eccentric and oblique axis spinning is consistent with the experimental results of uniaxial symmetric spinning shown in Figure 3 (c).

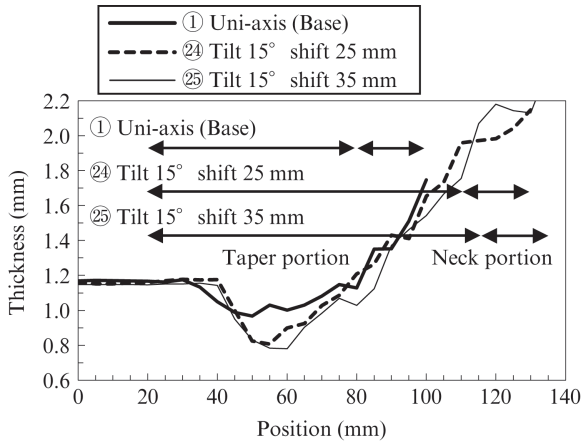

Fig. 9 Thickness distribution of spinning formed specimen

4.2 Temperature Elevation in Eccentric and Oblique Axis Spinning

Figure 10 shows the appearance of the samples of Steel A and Steel B formed by uni-axial symmetric spinning under Condition ① and eccentric and oblique axis spinning under Condition ㉕ in Table 3. Blueing (temper color) due to temperature elevation can be seen in the samples formed by eccentric and oblique axis spinning, and is particularly remarkable in Steel B. To investigate this phenomenon, the temperature during spinning forming was measured by attaching thermocouples TC10, TC20, TC30, TC40 and TC50 at positions 10 mm, 20 mm, 30 mm, 40 mm and 50 mm from the pipe end, respectively, as shown in **Fig. 11**. The

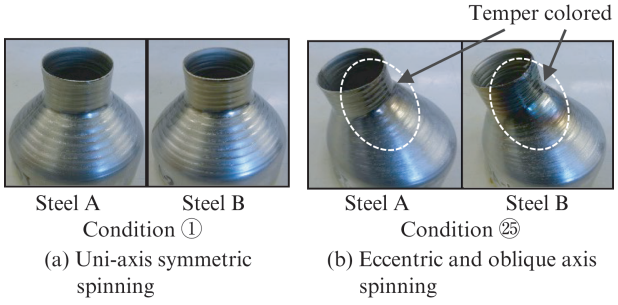

(a) Uni-axis symmetric spinning (b) Eccentric and oblique axis spinning

Fig. 10 Appearance of spinning formed specimen

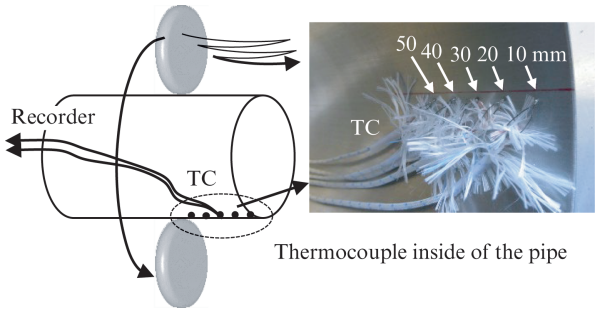

Fig. 11 Experimental method of temperature measurement during the spinning

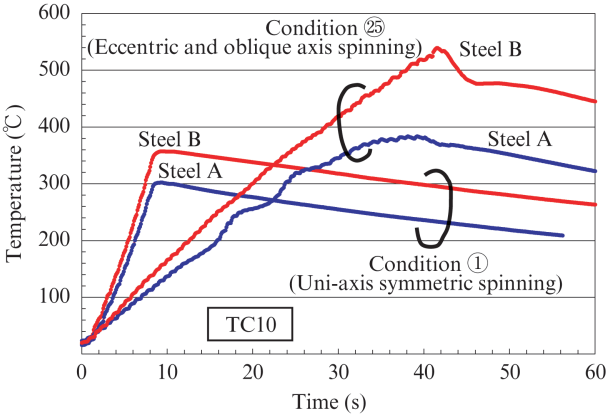

Fig. 12 Temperature change of specimen during spinning

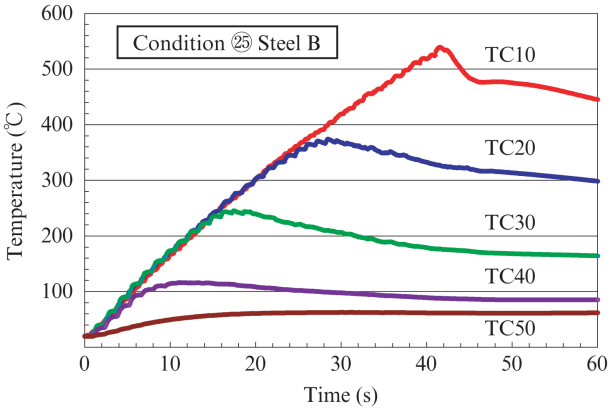

Fig. 13 Temperature change of specimen at each measuring point during eccentric and oblique axis spinning

temperature at the position 10 mm from the pipe end are shown in **Fig. 12**. The temperature elevation in eccentric and oblique axis spinning is larger than that in uni-axial symmetric spinning, and it is also larger in Steel B than in Steel A. In eccentric and oblique axis spinning of Steel B, which displayed remarkable blueing, the temperature reached 540°C or higher. **Figure 13** shows the temperatures at each of the measurement points in eccentric and oblique axis spinning of Steel B. A similar temperature elevation was observed at all measurement points immediately after the start of forming, but after forming from the far side to the pipe end was completed, the temperature elevation stopped in the order of TC50→TC40→TC30→TC20→TC10, then the temperature began to decrease. The highest temperature was reached at measurement point TC10, at 10 mm from the pipe end, where forming continued until the end. In uni-axial symmetric spinning, the forming time is short and the temperature is elevated rapidly, but in eccentric and oblique axis spinning, the temperature is elevated gradually because the forming time is long, but the achieved temperature is high due to the large final amount of deformation. The temperature condition during spinning is complicated, since it is related to frictional heating, processing heat (heat of plastic deformation), heat removal to the atmosphere or tools, heat conduction (transfer) to the unformed portion and chuck, and other factors. However, because the workpiece material is thin and the contact area with the tools is small, it can be thought that processing heat and released heat to the atmosphere are the temperature controlling factors. Since the amount of processing heat per weight is similar for the same target shape, temperature rise elevation is also approximately the same, independent of the sheet thickness. When the workpiece material thickness is large, a greater amount of heat is accumulated in this process. On the other hand, assuming the surface area is the same, the amount of released heat to the atmosphere is similar, but in thicker workpiece material, the amount of released heat is relatively small in comparison with the amount of accumulated heat. That seems to be because thicker Steel B (thickness: 1.51 mm, Steel A: 1.15 mm) reached a higher temperature.

4.3 Surface Defects by Eccentric and Oblique Axis Spinning

In the sample of Steel B formed by eccentric and oblique axis spinning, fine surface defects were observed in the area from the taper shoulder portion to the neck portion. The appearance and a cross section are shown in **Fig. 14**. These surface defects did not reach the other surface, and therefore seemed to be shallow cracks or folded wrinkles. Because the surface defects occurred in the blueing portion, where the achieved temperature was high, and the deformed structure around the defect was uniform (i.e., similar to that of normal area), they are thought to be related to the temperature elevation and some irregular uneven surface texture. Two-dimensional FEM simulation about the deformation of cross-section including initial defect was conducted in order to investigate the cause of the surface defect. An initial surface defect with an opening of 100 μm, a depth of 50 μm, and V-shaped

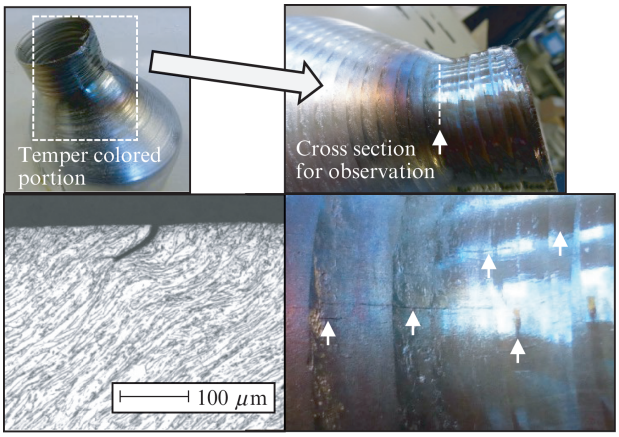

Condition ㉕ Steel B

Fig. 14 Fine clack defect at surface of eccentric and oblique axis spinning formed specimen

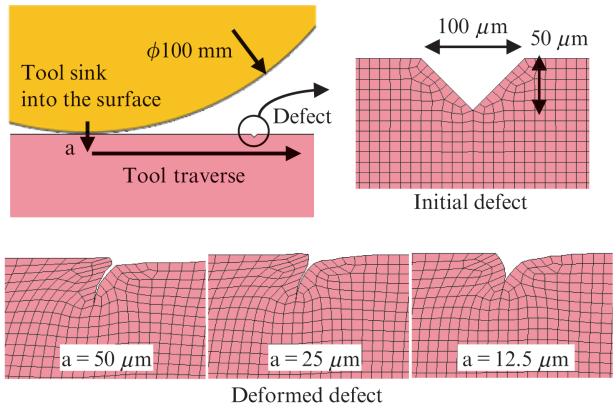

Fig. 15 Change of defect shape at spinning formed surface

bottom at an angle of 90° was given to the cross-section model as shown in **Figure 15**. The deformed defects after the roller tool (φ100 mm) used in spinning passed over the initial defect were compared between tool penetrations into the surface of 50, 25 and 12.5 μm. The initial surface defect did not disappear, but it deformed as its opening closed. The final defect in Figure 15 was similar to the cross section features of actual surface defect in Figure 14. However, no surface defect was observed on the initial pipe and the formed workpiece at each pass. This suggests that the surface irregularities that caused the surface defects might appear just before the end of the forming.

5. Conclusions

The following findings were obtained through experiment and FEM simulation about spinning forming.

In uni-axial symmetric spinning:

(1) Buckling at the pipe end occurs under a low tool rotation rate.

(2) Thickness reduction in the tapered shoulder portion is suppressed by an increased number of tool passes, and on the other hand, buckling tends to occur at the pipe end by a decreased number of tool passes.

(3) Thickness reduction in the tapered shoulder portion is suppressed by the reduction of the tapered shoulder angle.

(4) The results of FEM simulation were in good agreement with the experimental results, suggesting that FEM simulation could predict thickness distribution and buckling in spinning forming.

In eccentric and oblique axis spinning:

(5) The thickness reduction in the tapered shoulder portion is larger in eccentric and oblique axis spinning than in uniaxial symmetric spinning under the same diameter reduction ratio.

(6) The temperature elevation in the neck portion is larger in eccentric and oblique axis spinning than in uniaxial symmetric spinning.

(7) The closer to the pipe end a measuring point, the higher the temperature.

(8) The temperature in the neck portion gets higher as the thickness of a row pipe increases.

(9) In the eccentric and oblique axis spinning of Steel B (thickness 1.51 mm), the temperature at the pipe end reached 540°C at its maximum.

(10) Small surface defects occurred in the eccentric and oblique axis spinning of Steel B, but they did not penetrate the wall of the formed pipe.

(11) The results of FEM simulation suggest that a surface dent which occurs during spinning forming could cause the surface crack.

References

1) Takahashi, Y.; Kihara, S.; Nagamachi, T.; Mizumoto, H.; Nakata, Y. Effects of Forming Condition on Wrinkling in Neck of Pipe End. Journal of the JSTP. 2010, vol. 51, no. 591, p. 348–352.
2) Takahashi, Y.; Kihara, S.; Nagamachi, T.; Mizumoto, H.; Nakata, Y. Effects of Forming Conditions on Wrinkling in Necking of Tube End. Materials Transactions. 2011, vol. 52, no. 1, p. 31–36.
3) Takada, Y.; Takahashi, Y. Spinning Technology. Journal of the JSTP. 2013, vol. 54, no. 628, p. 403–407.
4) Ando, A.; Karino. S. Influence of Forming Conditions on Thickness Decrease of Welded Stainless Steel Pipes in Spinning Formin. Nissin Steel Technical Report. 2013, no. 94, p. 17–24.
5) Murata, M.; Muta, R. Effect of Thickness on Accuracy of Tube Spinning. Journal of the JSTP. 2001, vol. 42, no. 481, p. 124–128.
6) Yao, J.; Murata, M. An experimental study on spinning of taper shape on tube end. Journal of Materials Processing Technology. 2005, no. 166, p. 405–410.
7) Shindo, K.; Ishigaki, K.; Kato, K.; Irie, T. Development of the New Spinning Technology of Tube. Proceedings of the 50th Japanese Joint Conference for the Technology of Plasticity, JSTP, Fukuoka. 1999, p. 173–174.
8) Irie, T.; Yoshioka, S.; Imai, T. Development of the New Spinning

Technology of Tube-Second report-. Proceedings of the Japanese Spring Conference for the Technology of Plasticity, JSTP, Tokyo. 2000, p. 465–466.
9) Iguchi, T.; Yoshitake, A.; Irie, T.; Morikawa, A. Numerical Simulation and Development of Tube Spinning Process for Exhaust System Components of Motor Vehicles. Materials Processing and Design. Modeling, Simulation and Application, NUMIFORM. 2004, p. 1077–1082.
10) Ozaki, Y.; Ishiwatari, A.; Tamai, Y. CAE Analysis of Effects of Conditions in Spinning Forming on Shape Defects of Automotive Exhaust Part. Transaction of Society of Automotive Engineers of Japan. 2017, vol. 48, no. 2, p. 555–561.
11) Ozaki, Y.; Ishiwatari, A.; Tamai, Y.; Hiramoto, J. CAE Analysis of Effects of Conditions in Spinning Forming on Shape Defects of Automotive Exhaust Part. Journal of Society of Automotive Engineers of Japan. 2018, vol. 72, no. 10, p. 89–94.